A COMPARISON BETWEEN TRANSIENT HEAT TRANSFER MEASUREMENTS USING TLC AND IR THERMOGRAPHY

Stefan Brack*, Rico Poser and Jens von Wolfersdorf
Institute of Aerospace Thermodynamics (ITLR)
University of Stuttgart
Stuttgart, D-70569
*Email: Stefan.Brack@itlr.uni-stuttgart.de

ABSTRACT

Narrowband thermochromic liquid crystals (TLCs) and infrared thermography (IRT) are compared in the context of spatially resolved and transient heat transfer measurements. For accurate measurements the TLC coating was calibrated with a stationary method before the experiment. The IRT-camera was in-situ calibrated with a surface thermocouple.

A good agreement on temperature was achieved for both methods.

The TLC data as a single point measurement was evaluated for a time-independent heat transfer coefficient h_{TLC}. The surface temperature history measured with the IRT-camera enables an additional evaluation for a time-dependent $h_{\mathrm{CF}}(\mathrm{t})$.

In the case of one-dimensional heat conduction situations and late TLC indications h_{TLC} and $h_{\mathrm{CF}}(\mathrm{t})$ agree well after the first 10 s of the experiment.

An investigation of the heat transfer in the wake region of a vortex generator illustrated the influence of lateral conduction. This effect is not taken into account by any method and leads to greater differences between h_{TLC} and $h_{\mathrm{CF}}(\mathrm{t})$.

NOMENCLATURE

Acronyms

CCD	Charge-coupled device
IRT	Infrared thermography
TLC	Thermochromic liquid crystal
VG	Vortex Generator

Greek symbols

ΔT	Temperature difference
$\Delta\mathrm{t}$	Time difference
ε	Emittance
Φ	Radiation
ρ	Density
ϱ	Reflectance
τ	Transmittance

Roman symbols

c	Specific heat capacity
d	Diameter
h	Heat transfer coefficient
k	Wall thermal conductivity
L	Plate thickness
Re	Reynolds number
T	Temperature
t	Time

Subscripts

0	Initial
amb	Ambient
atm	Atmosphere
C	Coating
Cam	Camera
CF	Cook-Felderman
d	Duration
h	Hydraulic
i	Indication
QS	Quasi-stationary
ref	Reference
S	Surface
TC	Thermocouple
W	Window
∞	Ambient

INTRODUCTION

Internal blade cooling development of modern gas turbines is still driven by experimental investigations of the heat transfer. As a result of the complex-shaped cooling geometries like for example skewed ribs, pin fins or swirl chambers, measurement techniques delivering distributions of surface heat transfer coefficient are state of the art.

Since the heat transfer coefficient

$$h = \frac{\dot{q}_{\mathrm{S}}}{T_{\mathrm{ref}} - T_{\mathrm{S}}} \tag{1}$$

is an only indirectly measureable quantity it is often evaluated with the aid of spatially resolved surface temperature T_{S} measurements in combination with

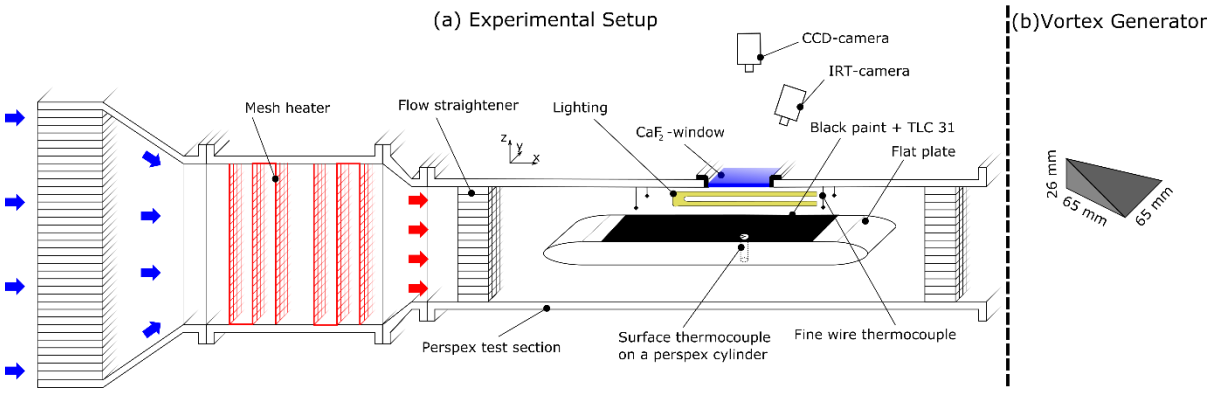

FIGURE 1: Experimental setup

transient experiments. In Eqn. (1) $\dot{q}_S$ represents the surface heat flux and T_{ref} the fluid reference temperature.

One widely spread possibility to measure the surface temperature T_S is a thermochromic liquid crystal (TLC) coating. In literature narrowband TLC [1-4] as well as wideband TLC [5-7] are applied to this type of experiments. Narrowband TLC with the indication band of about 1 K achieve accurate single point temperature measurements at each position in a transient experiment but result in necessary assumptions for the evaluation method [8]. A main assumption also discussed in section TLC DATA EVALUATION is a time-independent h.

Wideband TLC indicate over a broader temperature range but suffer from the increasing uncertainty for broader temperature bands [9].

Another surface temperature measurement technique also applicable to this type of experiments is the infrared thermography (IRT) [10-13]. The recent advances in the IRT-systems lead to systems with high accuracy, high spatial resolution and temporal resolution [13]. The main advantages of the IRT-systems compared to the TLC are the detection of the full T_S-history, a broad temperature range and a relative insensitivity of the camera angle [14]. The main disadvantages are the necessity of an in-situ calibration for the measurement of absolute temperature levels, special optics with a high IR transmittance and the possible influence of the actual overall thermal situation.

In this study heat transfer measurement results evaluated with the aid of two different surface temperature measurement techniques are discussed. On the one hand the T_S measurement with narrowband TLC and on the other hand the measurement with an IRT-camera. The experimental setup offers the possibility that both techniques measure simultaneously the same surface during one experiment.

For comparison two different heat transfer situations are evaluated. First the heat transfer on a flat plate and second the heat transfer in the wake region of a vortex generator.

The measurement data from the two temperature measurement methods is evaluated in different ways. First with the transient TLC-method based on an analytical solution for a one-dimensional heat conduction process inside a semi-infinite wall [15]. Second with the Cook-Felderman method calculating the time dependent surface heat flux $\dot{q}_S$ with the T_S-history [16]. Finally, the IRT-data are evaluated similar to the TLC-method for each value of the detailed T_S-history.

EXPERIMENTAL SETUP

FIGURE 1 (a) shows a schematic diagram of the experimental setup primarily designed for transient TLC experiments and modified to additionally measure the surface temperature with an IRT-camera.

The air from the ambient is sucked through the dust filter and heated up with the aid of the mesh heater. Six fine-wire meshes (three in series) connected to a power supply of 9.75 kW result in a sudden change of the fluid temperature and a homogeneous temperature distribution over the complete cross section.

Directly downstream of the mesh heater follows the perspex test section with a constant cross section of 120 mm times 150 mm.

The investigated heat transfer surface is part of a flat plate located in the symmetry plane of the test section. The test section as well as the flat plate are made of perspex with the material properties listed in TABLE 1.

In order to achieve acceptable measurement times complying the semi-infinite wall assumption the flat plate's thickness L is 30 mm.

The flat plate splits the test section into two sub-channels with a hydraulic diameter d_h of 80 mm each.

A 5 mm thick CaF_2-window kept by an aluminum frame offers an optical access for the IRT-camera as well as the CCD-camera. With a transmittance above 95% in the range of $1-5$ µm the CaF_2-window ensures a strong measurement signal and low influence of the radiance of the surrounding.

Two fine-wire thermocouples in front and downstream the window measured the freestream temperature applied as T_{ref}. A stationary calibration with a dry block calibrator (AMETEK™ RCT-159B) reduced the uncertainty of the thermocouples to 0.1 K. The wire diameter d_{TC} of the thermocouples was 0.08 mm.

A NI-USB6218 data acquisition system combined with an I.E.D. thermocouple amplifier measured the thermocouple's voltages at a sampling rate of 50 Hz.

Above the test section a SONY DFW-X710 digital video camera with a frame rate of 15 Hz filmed the TLC color play uniformly illuminated by two 35 W warm white (3000 K) fluorescent lamps. For all experiments the surface of the flat plate was coated with two thin layers of black paint layer and TLC.

The calibration of the TLC indication temperature T_{TLC} delivered a value of 31.91 °C (Hallcrest R31C1W). Poser et al. [17] discuss the applied stationary calibration procedure in detail.

A FLIR SC7600 IRT-camera at a frame rate of 25 Hz detected the surface radiation of the flat plate. The camera detector is sensitive in the spectral range from 1.5 µm to 5.1 µm and has a noise equivalent temperature difference value below 25 mK.

In order to in-situ calibrate the IRT-camera the flat plate includes one cylindrical sensor mount in the field of view. A 0.013 mm thick thin film surface thermocouple (OMEGA CO-2) glued on a perspex cylinder filled the sensor mount. Equally to the fine-wire thermocouples the thin film thermocouples was calibrated with the dry block calibrator.

With the vortex generator (VG) shown in FIGURE 1 (b) a variation of the investigated heat transfer pattern was realized. Mounting the VG on the top of the flat plate and in front of the CaF_2-window leads to a locally strong varying heat transfer. The heat transfer variation is induced by the longitudinal vortex systems described by Henze et al. [18].

TLC-DATA EVAULATION

One of the most widely spread transient evaluation methods bases on a T_{S}-change triggered by a sudden change in T_{ref} and starting at thermal equilibrium T_0. Filming the color change of the narrowband TLC delivers an accurate measurement of the time duration t_i for reaching $T_{\mathrm{TLC}} = T_{\mathrm{S}}|_{t_{\mathrm{i}}}$.

TABLE 1: Material Properties of perspex

Property	Value	Unit
Density ρ	1190	$\mathrm{kg/m^3}$
Specific heat capacity c	1470	$\mathrm{J/kgK}$
Thermal conductivity k	0.19	$\mathrm{W/mK}$

Using the data of T_0, $T_{\mathrm{ref}}(t)$, T_{TLC} and t_{i} a time-independent h_{TLC} can be calculated.

For a series of step changes $\Delta T_{j,j-1}$ in $T_{\mathrm{ref}}(t)$ and a one-dimensional heat conduction situation within a semi-infinite wall of constant material properties the following evaluation equation

$$T_S - T_0 = \sum_{j=1}^{N}\left[1 - \mathrm{e}^{\frac{h^2(t-t_j)}{\rho c k}} \times \mathrm{erfc}\left\{\frac{h\sqrt{t-t_j}}{\sqrt{\rho c k}}\right\}\right]\Delta T_{j,j-1} \quad (2)$$

is valid.

Limiting the duration of the experiment t_{d} with

$$t_{\mathrm{d}} < \frac{1}{16}\left[\frac{L}{2}\right]^2\frac{\rho c}{k} = 129.5\ \mathrm{s} \quad (3)$$

ensures the compliance of the semi-infinite wall assumption [16].

Beside Eqn. (2), used in this publication, other analytical solutions for different experimental situations exist. Kwak et al. [19] discuss the modelling of the T_{ref}-history with various functions like an exponential raise or an n-th order polynomial.

Kingsley-Rowe et al. [20] present an analytical empirical approach to consider lateral conduction effects which is extended to three dimensions and an exponential T_{ref}-change by Brack et al. [21].

Von Wolfersdorf [22] derives a solution considering the lateral conduction effects induced by a spatially varying T_{ref}-history.

More complex and computationally expensive evaluation methods apply the TLC measurement as an input for numerical simulations [6, 7, 23, 24].

IRT-DATA EVALUATION

The measured thermal radiation of IRT-camera Φ_{Cam} used in the experimental setup is not only influenced by the radiation of the heat transfer surface Φ_{S}. A radiation balance also sketched in FIGURE 2 shows an additional influence of the hot ambient inside the channel (channel walls) $\Phi_{\mathrm{amb,h}}$, the hot atmosphere inside the channel $\Phi_{\mathrm{atm,h}}$, the cold atmosphere around the channel $\Phi_{\mathrm{atm,c}}$, the cold ambient $\Phi_{\mathrm{amb,c}}$ and the window Φ_{W}. Combining the radiation terms with the corresponding transmittance τ and reflectance ϱ leads to the following radiation balance equation

$$\Phi_{\mathrm{Cam}} = \Phi_{\mathrm{atm,c}} + \tau_{\mathrm{atm,c}}\left[\varrho_{\mathrm{W}}\Phi_{\mathrm{amb,c}} + \Phi_{\mathrm{W}} + \tau_{\mathrm{W}}\left\{\Phi_{\mathrm{atm,h}} + \tau_{\mathrm{atm,h}}(\varrho_S\Phi_{\mathrm{amb,h}} + \Phi_{\mathrm{S}})\right\}\right]. \quad (4)$$

The varying terms in Eqn. (4) are $\Phi_{\mathrm{atm,h}}$, $\Phi_{\mathrm{amb,h}}$ and Φ_{S}. The values of the other terms can be regarded as constant over t_{d}.

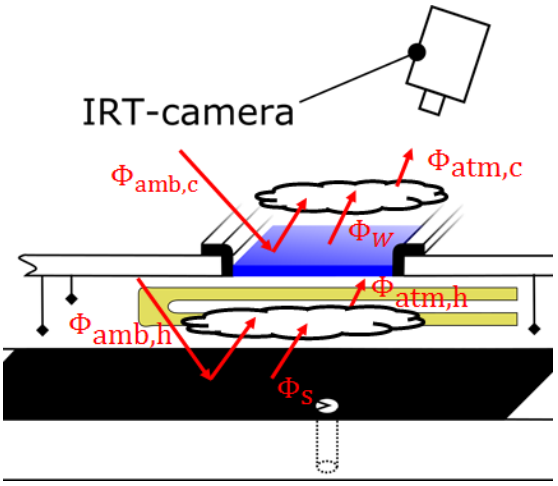

FIGURE 2: Radiation Balance

$\Phi_{atm,h}$ is negligible because of the thin hot air layer thickness of 60 mm leading to $\tau_{atm,h} \approx 1$ [25].

The influence of $\Phi_{amb,h}$ depends on ϱ_S. Using the Kirchhoff laws, one reaches the following relationship between the emittance of the surface ε_S and the reflectance ϱ_S [25]:

$$\varepsilon_S + \varrho_S = 1 \tag{5}$$

Necessary measurements of the band emittance of the coating $\bar{\varepsilon}_S$ were performed with the IRT-camera in a climate chamber for two different ambient temperatures $T_\infty = 5\,°C$ and $20\,°C$. The black paint plus TLC coating were sprayed on a liquid cooled or heated copper bar. A comparison of the copper bar temperature and the measured temperature with the IRT-camera delivered a temperature-dependent $\bar{\varepsilon}_S$ of the coating.

As FIGURE 3 shows, $\bar{\varepsilon}_S$ reaches a constant value of 0.9 for large temperature differences between the coating temperature T_C and T_∞. For small temperature differences $\bar{\varepsilon}_S$ decreases as the measurement uncertainty increases.

Concluding the term $\varrho_S \Phi_{amb,h}$ in Eqn. (4) is neglected simplifying Eqn. (4) to

$$\Phi_{Cam} = \Phi_{atm,c} + \tau_{atm,c}\left[\varrho_W \Phi_{amb,c} + \Phi_W + \tau_W \Phi_S\right]. \tag{6}$$

Eqn. (6) still shows the necessity of an in-situ calibration of the IRT-camera signal because of the unknown but constant quantities $\Phi_{atm,c}$, $\tau_{atm,c}$, ϱ_W, $\Phi_{amb,c}$ and Φ_W. The local IRT-data at the surface thermocouple positions and the surface thermocouple data itself lead to an in-situ calibration curve for the IRT-data of the complete field of view.

The measurement of the complete T_S-history offers the possibility to evaluate the IRT-data in two different ways. First regarding every point in time as a single point measurement like the TLC-data and calculate an h with Eqn. (2). This evaluation directly

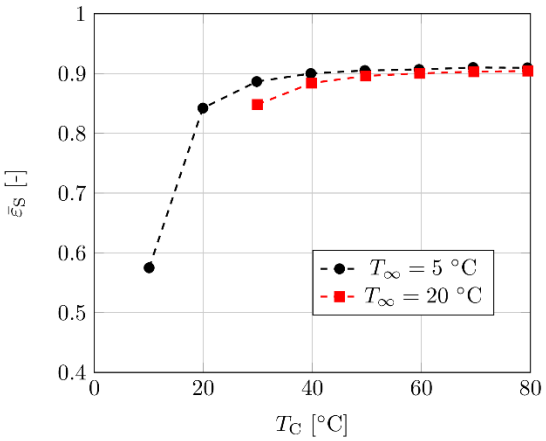

FIGURE 3: Band emittance of black paint and TLC coating

combines $T_{ref}(t)$ and T_S information in order to determine the in the following so called h_{QS}(t).

The second evaluation method applies the Cook-Felderman method derived by Schultz and Jones [16] calculating the local surface heat flux $\dot{q}_S(t)$ using T_S(t) as boundary condition for the conduction problem.

Identically to Eqn. (2) the Cook-Felderman method is valid for one-dimensional heat conduction problems with constant material properties inside a semi-infinite wall. This leads to the analytical solution for the surface heat flux

$$\dot{q}_S(t) = \sqrt{\frac{\rho c k}{\pi}}\left[\frac{T_S(t)}{\sqrt{t}} + \frac{1}{2}\int_0^t \frac{T_S(t) - T_S(\delta)}{(t-\delta)^{3/2}}\,d\delta\right]. \tag{7}$$

Solving the integral in Eqn. (7) numerically with a piece-wise linear approximation of the T_S-history reduces Eqn. (7) to

$$\dot{q}_{S,CF}(t) = \frac{2\sqrt{\rho c k}}{\sqrt{\pi}} \times \sum_{j=1}^{n} \frac{T_S(t_j) - T_S(t_{j-1})}{\sqrt{t_n - t_j} + \sqrt{t_n - t_{j-1}}}. \tag{8}$$

The heat transfer coefficient $h_{CF}(t)$ is calculated in a post processing step with

$$h_{CF}(t) = \frac{\dot{q}_{S,CF}}{T_{ref}(t) - T_S(t)}. \tag{9}$$

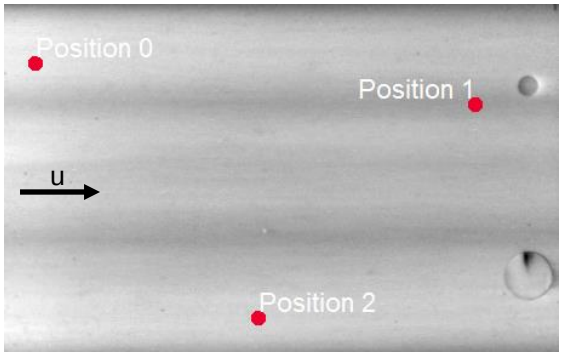

FIGURE 4: Evaluation positions flat plate experiment

A main advantage of the Cook-Felderman method is that the data evaluation for $\dot{q}_{S,CF}$ is independent from T_{ref}.

DATA COMPARISON

In order to compare the spatially resolved data received from the CCD-camera and the IRT-camera a previous camera calibration for distortion was performed with LabVIEW VISION™. A printed calibration grid filmed with both cameras delivered the information to consider the distortion for every frame and to define a common coordinate system.

RESULTS

The following section presents the results of two different heat transfer situations evaluated with the TLC-data as well as the IRT-data. The first part discusses the influence of the TLC indication time First a flat plate experiment with two different sudden fluid temperature changes illustrates the influence of the TLC indication time t_i. Therefore the results of two different sudden changes of T_{ref} are presented. A small variation of T_{ref} ($\Delta T_{ref} = 19$ K) leads to a relatively late TLC indication and strong variation of T_{ref} ($\Delta T_{ref} = 50$ K) leads to a relatively early TLC indication. The corresponding results are labeled with "Slow" and "Fast".

The second part deals with the influence of lateral conduction on all discussed evaluation methods. Therefore a VG was used to induce strong local variations in the heat transfer.

All experiments were performed at the same sub-channel Re number of 80,000.

Indication time – Flat plate experiment

The greyscale picture in FIGURE 4 illustrates the T_S-distribution 20 s after the beginning of the experiment (dark – low temperatures, bright – high temperatures). The red dots mark the three local evaluation positions.

In FIGURE 5 T_S is plotted against t for the evaluation points and the slow experiment. Besides the measured T_S-histories (IRT) additionally the calculated T_S-histories (TLC) are plotted. The calculated temperature histories were determined

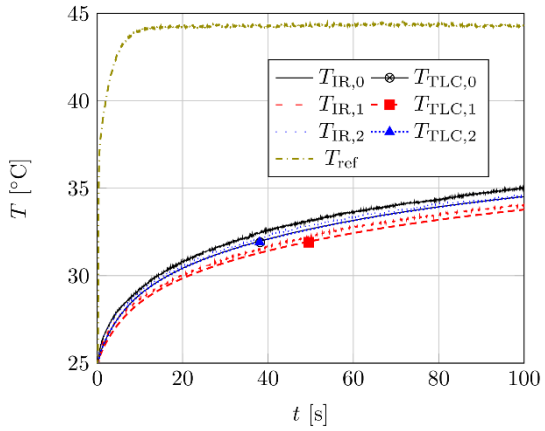

FIGURE 5: Temperature histories and TLC indication for the slow flat plate experiment

with Eqn. (2) and the received h from the TLC data at indication.

Independent of measurement or calculation all T_S-histories show the same shape. However the absolute values deviate as t_i deviates. Thereby t_i for the IRT-measurements was determined as the time point where the IRT-temperature equals the calibrated TLC-temperature.

TABLE 2 lists for the two experiments (slow and fast) the indication time t_i and includes the temperature deviation $T_{S,IR} - T_{TLC}$ for t_i between the IRT-data and the TLC-data.

The slow experiment leads to large time lags between both T_S measurement techniques. The maximum deviation is 6.53 s for Position 0. But with respect to the temperature difference $T_{S,IR} - T_{TLC}$, these time lags are a result of the measurement uncertainties. As the gradient of T_S is low for late indications, also small differences between both measurement techniques lead to larger time lags. This fact is confirmed with the results of the fast experiment.

Heat transfer – Flat plate experiment

In FIGURE 6 the determined heat transfer coefficients h are plotted against t for the different evaluation methods and the slow experiment. The

TABLE 2: Local Comparison between TLC and IRT

Pos.	Exp.	t_i [s] TLC	IRT	$[T_{S,IR} - T_{TLC}]$ [K] for t_i^{TLC}
0	Slow	38.17	31.64	+0.49
	Fast	4.22	3.85	+0.34
1	Slow	49.56	44.16	+0.29
	Fast	5.38	5.25	−0.05
2	Slow	38.05	35.48	+0.19
	Fast	4.31	4.37	+0.05

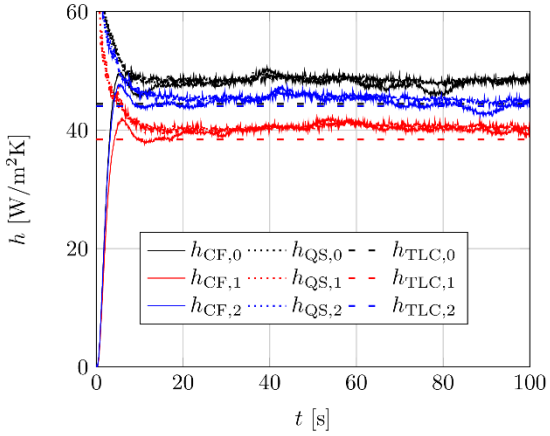

FIGURE 6: h-history for the slow flat plate experiment

assumption of a time-independent h_{TLC} for the TLC-method leads to a constant value.

All evaluation methods show an approximately constant h in the same range for evaluation times greater than 20 s. Up to 20 s the results differ in value and temporal evolution.

h_{QS} tends to infinity while h_{CF} starts at a value of zero. Additionally h_{CF} reaches the later nearly constant value with a small overshoot.

FIGURE 7 shows the time-resolved results of $\dot{q}_{\mathrm{S}}$ plotted against the driving temperature difference $T_{\mathrm{ref}} - T_{\mathrm{S}}$ of the heat transfer. As a result of the assumption of a time-independent h_{TLC} the surface heat flux $\dot{q}_{\mathrm{S,TLC}}$ is linear dependent on the driving temperature difference.

Conversely $\dot{q}_{\mathrm{S,QS}}$ increases first, reaches then a constant value before showing also a linear dependency from the driving temperature difference.

First $\dot{q}_{\mathrm{S,CF}}$ reveals only small values up to the temperature difference of about 10 K. Afterwards $\dot{q}_{\mathrm{S,CF}}$ increases nearly linear before changing the slope again.

FIGURE 8 shows the h-histories for the fast flat plate experiment. The deviation between h_{CF} and h_{TLC} is larger compared to the slow experiment.

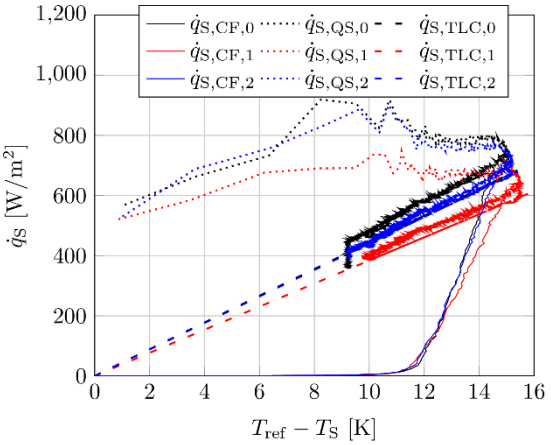

FIGURE 7: $\dot{q}_S$ plotted against $T_{\mathrm{ref}} - T_S$ for the slow flat plate experiment

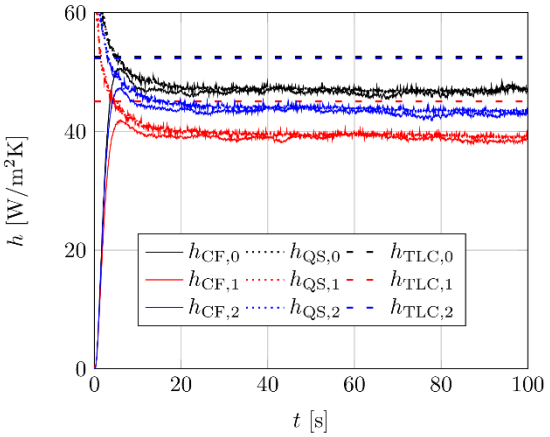

FIGURE 8: h-history for the fast flat plate experiment

The heat transfer coefficients h_{CF} evaluated with the IRT-data are again in a similar range and the history shows the same shape as for the slow flat plate experiment (see also FIGURE 6).

However a larger difference between both experiments can be seen for h_{TLC}. All h_{TLC}-values calculated with the data of the fast experiment are higher than in the case of the slow experiment.

Heat Transfer – Vortex generator experiment

The evaluation methods presented are only valid in the case of a one-dimensional heat conduction situation nearly achieved by the flat plate experiments. Nevertheless these methods are often used to investigate heat transfer distributions with strong spatial variations. The resulting lateral conduction effects are not captured leading to errors. The following results give an impression of this effect.

FIGURE 9 shows the T_{S}-distribution in the wake region of a vortex generator 10 s after the beginning of the experiment. The strong variation in T_{S} directly illustrate the variation in the heat transfer. In the downwash regions of the vortex systems T_{S} increases faster than in the upwash regions.

As a result of the longitudinal vortex pairs one upwash region lies between two downwash-regions

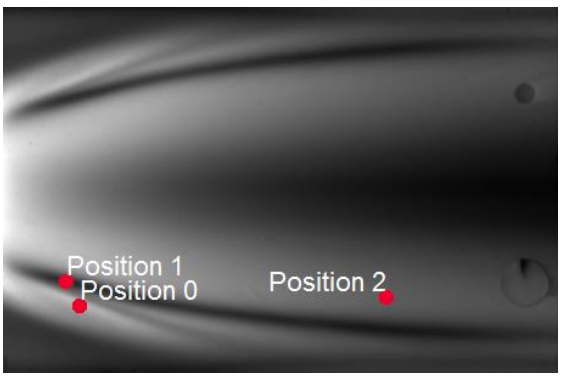

FIGURE 9: Evaluation positions for the vortex generator experiment

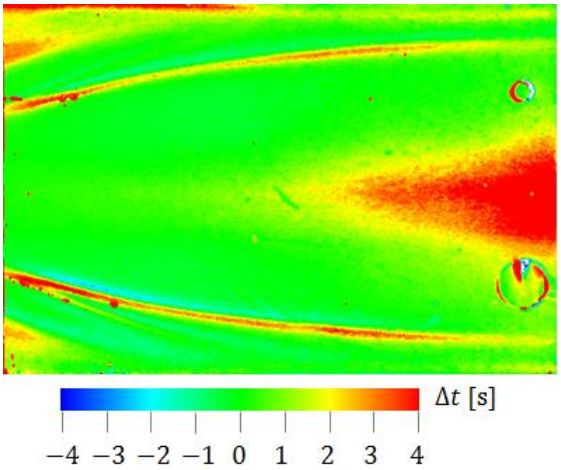

FIGURE 10: Contour plot of the t_i difference between TLC and IRT-data

and leads to strong lateral temperature gradients and lateral conduction effects.

A contour plot of the t_i difference

$$\Delta t = t_i^{IR} - t_i^{TLC} \quad (10)$$

between the TLC-data and the IRT-data is shown in FIGURE 10. Identically to the flat plate experiments late indication times lead to larger Δt. Furthermore, the contours of the time differences are well related to the local heat transfer coefficient distribution. This indicates the different effects of the lateral conduction processes on the individual evaluation method.

FIGURE 11 presents the h-histories for the three different evaluation points marked in FIGURE 9. The results of h_{TLC} strongly deviate from h_{QS} and h_{CF} expect for Position 2. This fact indicates a rather small influence of lateral conduction for Position 2. Additionally a constant h is reached after approximately 20 s for all evaluation methods at this position.

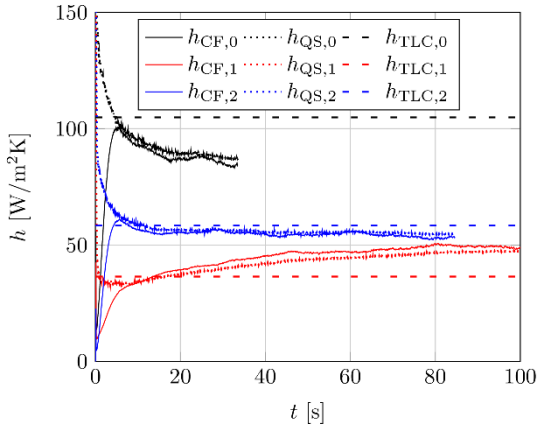

FIGURE 11: h-history for the vortex generator experiment

Position 1 is strongly influenced by lateral conduction as the conductive lateral heat flux is continuously towards this position from the surrounding positions. The heat transfer coefficient h_{CF} without considering lateral conduction never reaches a constant value and deviates from h_{TLC}.

The opposite situation is present for Position 0, where the lateral conduction heat flux is continuously away from this position to the surrounding positions due to the relatively high local heat transfer coefficient at this position.

CONCLUSION

Two surface temperature measurement techniques have been compared and used for the data evaluation of transient heat transfer experiments. The investigated surface was coated with narrowband TLC and additionally an IRT-camera measured the radiation of the surface.

As a result of the experimental setup the IRT-camera is not only influenced by the radiation of the investigated surface but also by the surrounding. A necessary in-situ calibration was performed with a surface thermocouple.

Both measurement techniques deliver the same surface temperatures in the range of the measurement uncertainties.

Initially, studies with low spatial variation of the heat transfer coefficient (flat plate) were performed. Afterwards the heat transfer in the wake region of a vortex generator with a strong spatial variation of the heat transfer coefficient was investigated.

The single point measurements of the narrowband TLC lead to time-independent heat transfer coefficients. The surface temperature histories of the IRT-camera are used to calculate the surface heat flux histories and delivered time-dependent heat transfer coefficients.

The results of the flat plate experiments showed the importance of the TLC indication time. Both evaluation methods agree well in the case of indication times approximately greater than 10 s. A earlier indication leads to a larger deviation between both methods.

For the experiment with a vortex generator larger deviations are detected depending on the evaluation position. These deviation results from the lateral conduction not taken into account by any of the applied data evaluation methods.

Positions strongly influenced by lateral conduction show a time-dependent heat transfer coefficient not reaching a constant value anymore. Therefore correction methods need to be applied and more elaborated data analysis methods considering the lateral conduction effects directly during data evaluation should be further developed.

REFERENCES

[1] Baughn, J.W. 1995: Liquid crystal methods for studying turbulent heat transfer, *Int. J. Heat Fluid Flow*, 1**6**, pp. 365-375.

[2] Kakade, V.U., Lock, G.D., Wilson, M., Owen, J.M., Mayhew, J.E. 2001: Multi-dimensional heat flux reconstruction using narrow-band thermochromic liquid crystal thermography, *Inverse Problem in Engineering*, **9**, pp. 537-559.

[3] Kakade, V.U., Lock, G.D., Wilson, M., Owen, J.M., Mayhew, J.E. 2009: Accurate heat transfer measurements using thermochromic liquid crystal. Part 2: Application to a rotating disc, *Int. J. Heat Fluid Flow*, **30**, pp. 365-375.

[4] Yan, W.M., Mei, S.C., Liu, H.C., Soong, C.Y., Yang, W.J. 2004: Measurement of detailed heat transfer on a surface under arrays of impinging elliptic jets by a transient liquid crystal technique*, Int. J. Heat and Mass Transfer*, **47**, pp. 5235-5245.

[5] Babinsky, H., Edwards, J.A., 1996: Automatic liquid crystal thermography for transient heat transfer measurements in hypersonic flow, *Experiments in Fluids*, **21**, pp. 227-236.

[6] Lin, M., Wang, T. 2002: A transient liquid crystal method using a 3-D inverse transient conduction scheme, *Int. J. Heat and Mass Transfer*, **45**, pp. 3419-3501.

[7] Wang, T, Lin, M. 2005: Flow and heat transfer of confined impingement jets cooling using a 3-D transient liquid crystal scheme, *Int. J. Heat and Mass Transfer*, **48**, pp. 4887-4903.

[8] Ireland, P.T:, Jones, T.V. 2000: Liquid crystal measurements of heat transfer and surface shear stress, *Meas. Sci. Technol.*, **11**, pp. 969-986

[9] Newton, P.J., Yan, Y., Stevens, N.E., Evatt, S.T., Lock, G.D., Owen, J.M. 2003: Transient heat transfer measurements using thermochromic liquid crystal. Part 1: An improved technique, *Int. J. Heat Fluid Flow*, **24**, pp. 14-22.

[10] Meola, C. Carlomagno, G.M. 2004: Recent advances in the use of infrared thermography*, Meas. Sci. Technol.*, **15**, pp. R27-R58.

[11] Bons, J. 2009: Transient method for convective heat transfer measurement with lateral conduction – Part I: Application to a deposit-roughened gas turbine surface, *J. Heat Transfer*, **131**, pp. 011301-1 -7.

[12] Bons, J., Fletcher, D., Borchert, B. 2009: Transient method for convective heat transfer measurement with lateral conduction – Part II: Application to an isolated spherical roughness element, *J. Heat Transfer*, **131**, pp. 011302-1 - 7.

[13] Helmer, D.B. 2014: Modified transient infrared methodology for leading edge impingement measurements, *ASME paper GT2014-25884*.

[14] Brauckmann, D., von Wolfersdorf, J. 2004: Infrared thermography with in-situ calibration using thermochromic liquid crystals applied to film cooling, *ASME paper GT2004-53855*.

[15] Metzger, D.E., Larson, D.E. 1986: Use of melting point surface coatings for local convection heat transfer measurements in rectangular channel flows with 90-deg turns, *J. Heat Transfer*, **108**, pp. 48-54.

[16] Schultz, D.L., Jones, T.V. 1973: Heat-transfer measurements in short duration hypersonic facilities, *AGARDograph*, **165**, pp. 1-157.

[17] Poser, R., von Wolfersdorf, J., Lutum, E., Semmler, K. 2008: Performing Heat Transfer Experiments in Blade Cooling Circuits Using a Transient Technique With Thermochromic Liquid Crystals, *ASME paper GT2008-50364*.

[18] Henze, M., von Wolfersdorf, J., Weigand, B., Dietz, C., Neumann, S. 2011: Flow and heat transfer characteristics behind vortex generators: a benchmark dataset, *Int. J. Heat Fluid Flow*, **32**, pp. 318-328.

[19] Kwak, J.S. 2008: Comparison of analytical and superposition solutions of transient liquid crystal technique, *J. Thermophysics*, **22**, pp. 290-295.

[20] Kingsley-Rowe, J.R., Lock, G.D., Owen, J.M. 2005: Transient heat transfer measure-ments using thermochromic liquid crystals: lateral-conduction error*, Int. J. Heat Fluid Flow*, **26**, pp. 256-263.

[21] Brack, S., Poser, P., von Wolfersdorf, J. 2016: An approach to consider lateral heat

conduction effects in the evaluation process of transient heat transfer measurements using TLC, *Int. J. Thermal Sciences*, **107**, pp. 289-302.

[22] von Wolfersdorf, J. 2007: Influence of lateral conduction due to flow temperature variations in transient heat transfer measurements, *Int. J. Heat and Mass Transfer*, **50**, pp. 1122-1127.

[23] Ryley, J., Mc Gilvray, M., Gillespie, D. 2014: Calculation of heat transfer coefficient distribution on 3D geometries from transient liquid crystal experiments, *ASME paper GT2014-26973*.

[24] Ling, J.P., Ireland, P.T., Turner, L. 2004: A technique for processing transient heat transfer, liquid crystal experiments in the presence of lateral conduction, *J. Turbomachinery*, **126**, pp. 247-258

[25] VDI Gesellschaft 2005: VDI-Wärmeatlas, *Springer Berlin Heidelberg*, pp. 1-1500.